

Coulomb charging energy of vacancy-induced states in graphene

V. G. Miranda,¹ Luis G. G. V. Dias da Silva,² and C. H. Lewenkopf¹

¹*Instituto de Física, Universidade Federal Fluminense, 24210-346 Niterói, RJ, Brazil*

²*Instituto de Física, Universidade de São Paulo, C.P. 66318, 05315-970 São Paulo, SP, Brazil*
(Dated: June 30, 2021)

Vacancies in graphene have been proposed to give rise to π -like magnetism in carbon materials, a conjecture which has been supported by recent experimental evidence. A key element in this “vacancy magnetism” is the formation of magnetic moments in vacancy-induced electronic states. In this work we compute the charging energy U of a single-vacancy generated localized state for bulk graphene and graphene ribbons. We use a tight-binding model to calculate the dependency of the charging energy U on the amplitudes of the localized wave function on the graphene lattice sites. We show that for bulk graphene U scales with the system size L as $(\ln L)^{-2}$, confirming the predictions in the literature, based on heuristic arguments. In contrast, we find that for realistic system sizes U is of the order of eV, a value that is orders of magnitude higher than the previously reported estimates. Finally, when edges are considered, we show that U is very sensitive to the vacancy position with respect to the graphene flake boundaries. In the case of armchair nanoribbons, we find a strong enhancement of U in certain vacancy positions as compared to the value for vacancies in bulk graphene.

PACS numbers: 73.22.Pr, 75.75.-c, 73.20.Hb

I. INTRODUCTION

Lattice defects have long been considered as an undesired presence in micro- and nanostructured devices. In many cases, they were deliberately avoided in the manufacturing processes since they modify the electronic and structural properties and are detrimental to electronic transport. More recently, this scenario has been changing as it has been shown that defects themselves can give rise to interesting physical phenomena in many condensed matter systems.

Graphene is one of the main platforms that is contributing to the growing interest in defective nanostructures. In addition to the remarkable and already thoroughly explored properties of clean graphene flakes,¹⁻³ experiments in graphene with vacancies reveal a new route to extend the plethora of fascinating aspects of this material.⁴⁻¹⁴

Some of the important discoveries pointed out by experiments in graphene with vacancies include the onset of magnetic behavior in a p -block system,^{6-8,14,15} signatures of the Kondo effect in the transport properties^{5,16,17} and the recently reported atomic charge collapse.¹²

Theory predicts that a vacancy originates a midgap state pinned at $E = 0$ and localized around the “vacancy site”.¹⁸⁻²⁰ This result is not exclusive to graphene and generalizes to all class of systems that can be represented by a bipartite-like hamiltonian with nearest neighbor interactions only²¹⁻²³. For such systems, a counting rule states that whenever an imbalance $N_I = |N_A - N_B| \neq 0$ between the number of constituents of the sublattices A and B exists, at least N_I states pinned at zero energy rise.^{19,21,24}

The picture described above relies on a simple model for the vacancy considering graphene π -band electrons only. This “ π -like” magnetism in graphene with va-

cancies has been reported experimentally recently,^{7,14} though its relevance for the vacancy-induced magnetism is a matter of a long debate in the DFT community.²⁵⁻³⁰ As we show next, our results reinforce the arguments in favor of the relevance of π -like magnetism in graphene with vacancies. Moreover, our arguments should be also valid for H adatoms, which can be described by an onsite scalar potential model.^{15,31}

A crucial aspect of the vacancy state and that is key for the understanding of the onset of magnetism, Kondo effect, and atomic collapse within this model is the charging energy of the vacancy state U . This parameter, also referred to as the “Hubbard-U”, encodes the local electron-electron Coulomb interaction of the vacancy state. As such, it leads to the spin splitting of the vacancy midgap state which is essential for the onset of magnetic behavior.³² In addition, the interplay between U and the hopping between the midgap state into the band states sets the condition for the onset of the Kondo effect.^{16,17,33} Moreover, it has been argued that the strength of U controls the vacancy charge and thus the critical coupling that determines the appearance of the atomic collapse.^{12,34}

The central focus of this work is the determination of the charging energy U of vacancies in graphene. We address this issue for bulk graphene as well as for graphene with edges. Previous analytical results on the wave function of a vacancy in bulk graphene^{18,19,27} and graphene with edges^{35,36} are extremely relevant for the results we present.

We recall that, for a single vacancy in bulk graphene, the vacancy wave function decays as $\sim 1/R$ with R being the distance from the vacancy site.^{18,19,27} This unusual behavior produces a non-normalizable wave function and hence the state is said to be quasi-localized with the degree of localization of the system decaying as the system

enlarges. This feature has led some authors to claim this would make U negligible for real samples.^{25,37}

It is well known that the presence of edges strongly modifies the electronic properties of graphene.^{38–44} When edges are introduced, important changes occur also on the vacancy state.^{35–37,45–48} Analytical accounts on the influence of edges in the vacancy-generated state in graphene have been recently put forward in Refs. 35 and 36. In these works, Deng and Wakabayashi studied the influence of edges on the vacancy localized state of a semi-infinite sheet³⁵ and graphene nanoribbons.³⁶ Interestingly, for the semi-infinite systems in the presence of an armchair edge, the vacancy state decays as $1/R^2$ and is thus normalizable.³⁵ When a zigzag edge is considered, the influence on the vacancy state depends on which sublattice the vacancy is created. Deng and Wakabayashi³⁵ find that if the vacancy and the edge sites belong to different sublattices, the vacancy causes no effect on the system zero energy states. In contrast, when both, edge and vacancy belong to the same sublattice, the vacancy yields a strongly distorted, non-normalizable zero-mode wave function around the vacancy site.³⁵ The case of vacancies in graphene nanoribbons was studied by the same authors in Ref. 36. They claim that a single-vacancy has no effect on the zero-energy states of zigzag-terminated edge ribbons, quantum dots, and armchair-terminated metallic ribbons. However, for armchair-terminated semiconductor ribbons, the vacancy generates a square-normalizable wave function pinned at $E = 0$.

Although the main focus of the present paper is the analysis of the charging energy of the vacancy-generated state in bulk graphene and graphene with edges, we also perform a systematic study of the vacancy-generated wave functions for graphene with edges. We combine analytical and numerical techniques to study how the properties of the vacancy state and its respective U is altered for different system sizes, edges and vacancy-edge-sites distance.

One of the most important results of this work is the derivation of an analytical expression for the computation of U . This result reveals that in addition to the *inter-site* contribution to the Coulomb charging at the vacancy, there is also a sizable *intra-site* contribution which has been so far overlooked. We note that, for bulk graphene, Ref. 33 finds that the $1/R$ decay of the midgap state leads to $U \sim (2\pi \ln L)^{-2}$, with L being the linear system size. Based on this scaling behavior, the authors estimate $U \sim 1$ meV for typical micron flake sizes. Here we confirm the U scaling predicted in Ref. 33, however our U estimates are orders of magnitude larger than their predictions and in line with RPA/Hubbard model calculations.^{37,49}

Very recently, scanning tunneling spectroscopy (STS) experiments¹⁴ in graphene deposited on a Rh foil report the appearance of spin-split states near vacancy sites, which is consistent with the presence of strong onsite interactions. The STS data show splittings of about 20

- 60 meV, which can, in principle, be directly compared to the effective U in their system (which depends on the effective dielectric constant at the vacancy site).

For graphene ribbons, U calculations have been performed for the case of armchair ribbons in Ref. 37. The authors find out that U is related to the inverse participation ratio (IPR) of the vacancy state, in agreement with the results we present below. However, their prediction that U vanishes for increasing ribbon widths³⁷ is not supported by our study. In this paper, we also perform a systematic study of the of the IPR and U of the vacancy states for different ribbon widths and edge-vacancy-sites distances, a study lacking in the literature to the best of our knowledge. Our results point that for some vacancy-edge-sites distances, U decreases with increasing ribbon widths and approaches the bulk estimates, however remaining close to ~ 1 eV even for real sample sizes, contrary to the vanishing U predicted elsewhere.^{25,33} We also find that there are some vacancy-edge-sites distance configurations for which a directionality effect of the vacancy wave function makes the IPR and U system-size independent, being a truly localized state. This is the second main contribution of our work.

The paper is structured as follows. In Sec. II, we present the tight-binding formalism used to obtain the vacancy wave functions and to derive the analytical expression of U . In Sec. III, we use the results of the previous section to obtain U estimates in bulk graphene for varying system sizes. In Sec. IV, we make a thorough study of the vacancy state in graphene armchair ribbons for different configurations. We calculate the IPR of the midgap states to quantitatively evaluate the degree of localization of such states. We finish the section addressing the issue of vacancies in the presence of zigzag and quantum dots with both zigzag and armchair edges and show that our main findings for the armchair edges seems to remain robust to the additional presence of zigzag edges. In Sec. V we evaluate U for armchair ribbons and show that U mimics the IPR behavior. Also, we show that our results hold irrespective if the ribbons are semiconducting or metallic. Finally, we present our concluding remarks in Sec. VI.

II. VACANCY-INDUCED MIDGAP STATES: WAVE FUNCTION AND CHARGING ENERGY

In this section, we present a single-orbital tight-binding model description of the midgap states due to a single vacancy in graphene monolayer systems. We then derive analytical expressions for the Coulomb charging energy for these localized states. For notation compactness, we consider the charging energy U in vacuum. If the graphene layer is in contact with another medium, the calculated U should be divided by the corresponding dielectric constant ϵ .

We describe single-particle spectrum and wave func-

tion using the model Hamiltonian given by

$$H = H_0 + V, \quad (1)$$

where V accounts for a single monovacancy and H_0 is the pristine graphene tight-binding Hamiltonian,¹ namely

$$H_0 = -t \sum_{\langle i,j \rangle} (|i\rangle\langle j| + \text{H.c.}) \quad (2)$$

where $t \approx 2.8$ eV is the nearest neighbor hopping integral, $|i\rangle$ corresponds to a p_z orbital placed at the i th site of the graphene honeycomb lattice with interatomic separation $a = 1.41$ Å, $\langle \dots \rangle$ restricts the sums to nearest neighbors sites.

There are several equivalent ways to account for the vacancy.^{16,35} For analytical calculations it is convenient to model a monovacancy placed at the site v by an on-site potential term, namely,

$$V = V_0|v\rangle\langle v| \quad (3)$$

and take the limit $|V_0/t| \gg 1$. Alternatively, one can also use

$$V' = t \sum_{\langle v,j \rangle} (|v\rangle\langle j| + \text{H.c.}), \quad (4)$$

which corresponds to turning off the hopping terms that connect the vacancy site v to its nearest neighbors. From the numerical point of view both models, V and V' , give the same results for the low-energy single-particle properties of the system.¹⁹ (This statement is also corroborated by the good agreement between our results and those of Ref. 35.)

The single-particle electronic properties of a system with an impurity can be analytically obtained from a T -matrix analysis.⁵⁰ The T -matrix for a Hamiltonian of the form $H = H_0 + V$ reads $T = V(1 - VG_0)^{-1}$, where $G_0 = (E + i\eta - H_0)^{-1}$ is the Green's function of the pristine graphene system. For $|V_0/t| \gg 1$, the T matrix reduces to⁵⁰

$$T(E) = -\frac{|v\rangle\langle v|}{\langle v|G_0(E)|v\rangle}. \quad (5)$$

In general, the system wave functions are obtained from the Lippmann-Schwinger equation, $|\psi\rangle = (1 + G_0T)|\psi^{(0)}\rangle$, namely

$$\psi_E(i) = \psi_E^{(0)}(i) - \frac{\langle i|G_0(E)|v\rangle}{\langle v|G_0(E)|v\rangle} \psi_E^{(0)}(v) \quad (6)$$

where $\psi_E^{(0)}(i) = \langle i|\psi_E^{(0)}\rangle$ is the unperturbed wave function amplitude at the site i , solution of $H_0|\psi_E^{(0)}\rangle = E|\psi_E^{(0)}\rangle$. The knowledge of $\langle i|G_0(E)|j\rangle$ allows one to analytically calculate $\psi_E(i)$.

Of particular interest is the vacancy-induced midgap state $|\psi_0\rangle$ at $E = 0$. However, for these states, a careful study of the $T(E \rightarrow 0)$ behaviour should be taken

into account since, depending on the particular geometry under interest, $T(E \rightarrow 0)$ diverges and the strategy outlined above to obtain the wave functions is not always straightforward.^{35,36} In addition, it has been found that if the system has a finite gap, as in a armchair semiconducting ribbon, the vacancy-induced midgap state becomes a truly bound state and the wave function is no longer given by the expression above (see, for instance, Refs. 35 and 36 for a thorough discussion of this case).

We also analyze the midgap state problem numerically. The vacancy breaks down the lattice translational invariance. For bulk systems, we find it convenient to introduce a supercell of dimension $N_{\text{tot}} = N \times M$ sites with periodic boundary conditions at its edges (the description of the unit cell for graphene nanoribbons is presented in Sec. IV). Figure 1 shows the superlattice geometry: the atomic lattice sites i are denoted by the labels (m, n, S) ,^{35,36} where n identifies the zigzag chain (with respect to the vacancy site) to which the site i belongs and m is the position of the i -th site within the chain, while $S = A$ or B is the sublattice index.

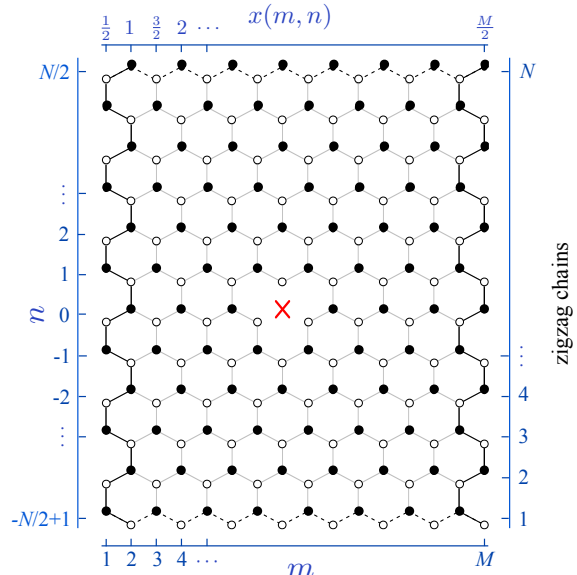


FIG. 1. Schematics of the supercell used in this work. The supercell is defined by $M/2$ “vertical” armchair chains and N “horizontal” zigzag ones. m is the discrete horizontal position with respect to the edge and n labels the horizontal zigzag chains starting from the one containing the vacancy, indicated by the cross.

The single-orbital graphene tight-binding Bloch basis is given by⁵¹

$$\chi_{\mathbf{k}j}(\mathbf{r}) = \frac{1}{\sqrt{N_{\text{sc}}}} \sum_{\mathbf{R}'} e^{i\mathbf{k}\cdot\mathbf{R}'} \phi(\mathbf{r} - \mathbf{t}_j - \mathbf{R}'), \quad (7)$$

where the sum runs over all N_{sc} supercells centered at \mathbf{R}' , \mathbf{t}_j gives the position of the j th carbon atom in the supercell, and $\phi(\mathbf{r})$ is the p_z orbital atomic wave function.

We take the limit of $N_{\text{tot}} = N \times M \gg 1$. Due to band folding, the Γ point gives a good representation of the first Brillouin zone of the supercell.^{52,53} For this reason, we restrict our calculation to $\mathbf{k}=0$ and drop the \mathbf{k} label from now on. The crystal electronic single-particle eigenstates are the solutions of $H\Psi_\nu(\mathbf{r}) = E_\nu\Psi_\nu(\mathbf{r})$ and read

$$\Psi_\nu(\mathbf{r}) = \sum_i \psi_\nu(i) \chi_i(\mathbf{r}), \quad (8)$$

where $\psi_\nu(i)$ is the ν th tight-binding wave function amplitude at the i th site and $\chi_i \equiv \chi_{\mathbf{k}=0,i}$. The midgap vacancy-induced state corresponds to $\nu = 0$. For later convenience, we introduce the envelope wave functions

$$\psi_\nu(\mathbf{r}_i) \equiv \frac{1}{\sqrt{\mathcal{A}}} \psi_\nu(i), \quad (9)$$

where \mathcal{A} is the supercell area. This approach allows us to calculate $\psi_0(\mathbf{r}_i)$ by direct diagonalization.

Let us now analyze the charging energy U corresponding to the Coulomb energy associated with a double occupation of the midgap state $|\psi_0\rangle$. It is rather tempting to use the envelope wave function $\psi_0(\mathbf{r})$ to evaluate U ,

namely³³

$$U = e^2 \int d^2r \int d^2r' \frac{|\psi_0(\mathbf{r})|^2 |\psi_0(\mathbf{r}')|^2}{|\mathbf{r} - \mathbf{r}'|}. \quad (10)$$

As shown below, this is the main contribution to the charging energy U due to the π orbitals. However we find another important contribution, which has been neglected so far.

The Coulomb energy associated to the double occupation of the vacancy-induced midgap state reads

$$U = e^2 \int d^3r \int d^3r' \frac{|\Psi_0(\mathbf{r})|^2 |\Psi_0(\mathbf{r}')|^2}{|\mathbf{r} - \mathbf{r}'|}, \quad (11)$$

where $\Psi_0(\mathbf{r})$ is the three dimensional wave function of the midgap state given by Eq. (8). U can then be expressed in terms of the tight-binding amplitudes as

$$U = \sum_{i,j,i',j'} \psi_0^*(i) \psi_0(j) \psi_0^*(i') \psi_0(j') W_{ij,i'j'}, \quad (12)$$

where the sums run over all N_{tot} atomic sites of the supercell and

$$W_{ij,i'j'} = e^2 \int d^3r \int d^3r' \phi^*(\mathbf{r} - \mathbf{t}_i) \phi(\mathbf{r} - \mathbf{t}_j) \frac{1}{|\mathbf{r} - \mathbf{r}'|} \phi^*(\mathbf{r}' - \mathbf{t}_{i'}) \phi(\mathbf{r}' - \mathbf{t}_{j'}). \quad (13)$$

Equation (12) does not include contributions from atomic orbitals located at different supercells, namely, $\mathbf{R} \neq \mathbf{R}'$. Since the Coulomb integral decreases rapidly as the orbital centers are separated, one only expects significant inter-supercell contributions from orbitals located at the edges of neighboring supercells. Those correspond roughly to a fraction $1/\sqrt{N_{\text{tot}}}$ of the supercell sites and can be safely ignored in the limit of $N_{\text{tot}} \gg 1$.

There is an extensive literature on the Coulomb integral $W_{ij,i'j'}$ in the context of generalizing the tight-binding ideas to obtain an atomistic total-energy method (see, for instance, Refs. 54–57 and references therein). The leading matrix elements⁵⁸ $W_{ij,i'j'}$ correspond to an intra-atomic (on-site) Coulomb repulsion matrix elements, where all orbitals belong to the same atom, and to inter-atomic (non-local) terms, where $i = j$ is in one atom and $i' = j'$ on another.

Accordingly, we decompose U as

$$U = U_1 + U_2, \quad (14)$$

where U_1 consists of intra-atomic Coulomb repulsion terms, while U_2 contains the inter-atomic ones.

Let us first consider U_1 , namely

$$U_1 = e^2 \int d^3r \int d^3r' \frac{|\phi(\mathbf{r})|^2 |\phi(\mathbf{r}')|^2}{|\mathbf{r} - \mathbf{r}'|} \sum_i |\psi_0(i)|^4, \quad (15)$$

where the Coulomb integral

$$U_{\text{orbital}} = e^2 \int d^3r \int d^3r' \frac{|\phi(\mathbf{r})|^2 |\phi(\mathbf{r}')|^2}{|\mathbf{r} - \mathbf{r}'|}, \quad (16)$$

can be evaluated, for instance, by an expansion of $|\mathbf{r} - \mathbf{r}'|^{-1}$ in spherical harmonics. Equation (16) represents the Hartree contribution to U . In the literature U_{orbital} was estimated to be ~ 17 eV for free standing graphene^{58,59} and, if screening effects from electrons of bands other than the π are taken into account, U_{orbital} reduces to ~ 8.5 eV.⁵⁹

Hence

$$U_1 = U_{\text{orbital}} \sum_i |\psi_0(i)|^4. \quad (17)$$

Let us now address U_2 , which is more conveniently expressed by changing the integration variables as $\mathbf{r} \rightarrow \mathbf{r} - \mathbf{t}_i$ and $\mathbf{r}' \rightarrow \mathbf{r}' - \mathbf{t}_j$, namely

$$U_2 = e^2 \sum_{i \neq j} |\psi_0(i) \psi_0(j)|^2 \int d^3r \int d^3r' \frac{|\phi(\mathbf{r})|^2 |\phi(\mathbf{r}')|^2}{|\mathbf{r} - \mathbf{r}' + \mathbf{t}_i - \mathbf{t}_j|}. \quad (18)$$

We write

$$U_2 = e^2 \sum_{i \neq j} \frac{|\psi_0(i)\psi_0(j)|^2}{|\mathbf{t}_i - \mathbf{t}_j|} \times \int d^3 r \int d^3 r' \frac{|\phi(\mathbf{r})|^2 |\phi(\mathbf{r}')|^2}{\sqrt{1 + \frac{|\delta \mathbf{r}|^2}{|\mathbf{t}_i - \mathbf{t}_j|^2} + \frac{2\delta \mathbf{r} \cdot (\mathbf{t}_i - \mathbf{t}_j)}{|\mathbf{t}_i - \mathbf{t}_j|^2}}}, \quad (19)$$

where $\delta \mathbf{r} = \mathbf{r} - \mathbf{r}'$. The orbital wave functions amplitudes $\phi(\mathbf{r})$ decay quickly for $r/a \gtrsim 1$ and more so the overlaps of the wave functions evaluated at distances $|\mathbf{r} - \mathbf{r}'|/a \gtrsim 1$. These observations suggest that U_2 can be approximated by the lowest order Taylor expansion in powers of $|\delta \mathbf{r}|/|\delta \mathbf{t}|$ of the square root at the r.h.s. of Eq. (19). This can be checked quantitatively by comparing with the exact values of the integral in Eq. (18).⁵⁸ We find that our approximation overestimates U_2 by about $\approx 10\%$, giving us confidence in the procedure.⁶⁰ Hence,

$$U_2 \approx e^2 \sum_{i \neq j} \frac{|\psi_0(i)|^2 |\psi_0(j)|^2}{|\mathbf{t}_i - \mathbf{t}_j|} \int d^3 r \int d^3 r' |\phi(\mathbf{r})|^2 |\phi(\mathbf{r}')|^2 \approx e^2 \sum_{i \neq j} \frac{|\psi_0(i)|^2 |\psi_0(j)|^2}{|\mathbf{t}_i - \mathbf{t}_j|}, \quad (20)$$

since the orbitals are normalized.

In the continuum limit, the sums in Eq. (20) can be changed to integrals and the site amplitudes can be replaced by an envelope wave function $\psi_0(\mathbf{r})$, leading to

$$U_2 \approx e^2 \int d^2 r \int d^2 r' \frac{|\psi_0(\mathbf{r})|^2 |\psi_0(\mathbf{r}')|^2}{|\mathbf{r} - \mathbf{r}'|}. \quad (21)$$

Many-body corrections to intra and inter atomic Coulomb repulsion terms of Eq. (13) have been calculated in Ref. 59. The latter uses Wannier-like orbitals projected in the p_z bands. This offers the advantage of separating the p_z contribution to the charge screening thereby accounting for the effective partial two-dimensional screening expected for the electrons in graphene.

In summary, the general expression for the Coulomb repulsion term U is given in terms of a three dimensional integral given by Eq. (11). We show how the latter can be cast into a two dimensional form proposed in the literature.³³ We also find an additional significant contribution to U that is proportional to U_{orbital} , given by Eq. (17).

III. U OF VACANCY-INDUCED LOCALIZED STATES IN BULK GRAPHENE

In this Section, we study the dependence of U with the system size. In order to reach our goal, we recall that the

wave function $\psi_0(\mathbf{r})$ of a localized state due to a single-vacancy in a clean bulk graphene monolayer reads²⁷

$$\psi_0(\mathbf{r}) = \frac{\mathcal{N}}{r} \sin \left[(\mathbf{K} - \mathbf{K}') \cdot \frac{\mathbf{r}}{2} - \theta_r \right] \times \cos \left[(\mathbf{K} + \mathbf{K}') \cdot \frac{\mathbf{r}}{2} - \frac{\pi}{3} \right], \quad (22)$$

where $\mathbf{r} = (x, y)$ is a coordinate vector with origin at the vacancy site, \mathcal{N} is the normalization constant, $\mathbf{K} = 2\pi/(3\sqrt{3}a)(-1, \sqrt{3})$ and $\mathbf{K}' = 2\pi/(3\sqrt{3}a)(1, \sqrt{3})$ denote the two inequivalent Dirac points in the first Brillouin zone, and $\theta_r = \arctan(x/y)$. Here, we consider finite systems with $N_{\text{tot}} = L \times L$ sites. Having an analytical expression for $\psi_0(\mathbf{r})$ is key for the study of systems with $L \gtrsim 10^2$ (or larger than 10^4 sites), since the computation time for exact diagonalization scales with L^6 .

Pereira and collaborators¹⁹ showed that for bulk graphene

$$\sum_i |\psi_0(i)|^4 \propto \frac{1}{(\ln L)^2}, \quad (23)$$

and thus

$$U_1 \propto \frac{U_{\text{orbital}}}{(\ln L)^2}. \quad (24)$$

Similarly, a rough estimate of U_2 can be obtained³³ by using the approximation $\psi_0(\mathbf{r}) \approx \mathcal{N}/r$. By normalizing the envelope wave function, the charging energy given by Eq. (21) reads $U_2 \propto e^2/\epsilon(\ln L)^{-2}$.

We use $\psi_0(\mathbf{r})$ given by Eq. (22) to estimate the charging energy U of the vacancy-induced state as a function of L . We insert the lattice wave function amplitudes $\psi_0(i) = \sqrt{\mathcal{A}}\psi_0(\mathbf{r}_i)$ in Eqs. (17) and (20) to numerically obtain U_1 and U_2 , respectively. To account for the effect of the substrate, we use $\epsilon = 4$, which is consistent with the value measured for graphene deposited on SiO_2 .⁶¹

Figure 2 gives U_1, U_2 , and $U_{\text{approx}} = U_1 + U_2$ as a function of L . We find that the dependence of the charging energy (in eV) with system size is accurately fitted by $U_{\text{approx}} = 0.32 + 82(\ln L)^{-2}$. Figure 2 shows that the U_2 estimates are almost an order of magnitude larger than those of U_1 .

The extrapolation of our results to graphene sheets with areas of about $1 \mu\text{m}^2$ (corresponding to $L \approx 10^7$ or 10^{14} sites), gives $U \approx 0.64\text{eV}$. This value is two orders of magnitude larger than the value predicted in Ref. 33, but consistent with the impurity splitting predicted for an impurity state due to a vacancy derived from the mean field Hubbard model³⁷ as well as from DFT calculations for small lattice sizes.⁶² Therefore, our results show that the π -like magnetism is not negligible in model systems with realistic sample sizes, in line with experimental evidences.^{7,14}

IV. GRAPHENE WITH EDGES

In this section we study the influence of the edges on the vacancy-induced states. More specifically, we present

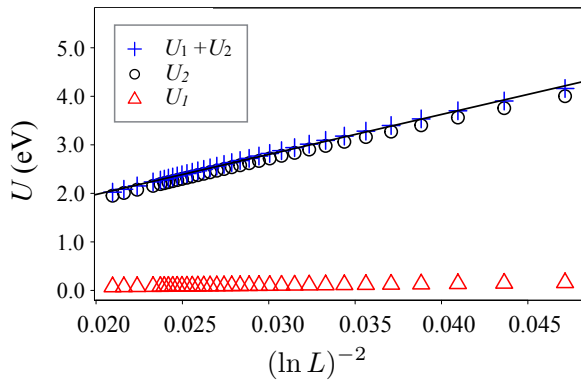


FIG. 2. (Color online) Scaling of the diagonal and off-diagonal charging terms U_1 and U_2 as a function of system size. Values are in eV.

a systematic study of the degree of localization and the charging energy U of the vacancy-induced states in armchair nanoribbons. We also provide a comparative analy-

sis with the cases of vacancies in zigzag nanoribbons and quantum dots. The main observation is that both localization and U are strongly dependent on the vacancy-edge distance.

A. Midgap state wave function in the presence of armchair edges

We follow two alternative approaches to study the characteristics of the vacancy-induced state: one that considers the analytical expression for the vacancy state derived in Ref. 36 and a numerical one which is based on the numerical diagonalization of the tight binding Hamiltonian described in Sec. II with armchair boundary conditions.

Let us consider, without loss of generality, a vacancy created at sublattice A. The wave function of $|\psi_0\rangle$ resides solely on sublattice B. In the notation presented in Sec. II, the expression for $\psi_0(m, n, S)$ presented in Ref. 36 is written as:

$$\psi_0(m, n, S) = - \sum_r I_r(n) \left[\cos \left(\frac{2\pi r(x_B(m, n) - x_0(m_0, 0))}{M+1} \right) - \cos \left(\frac{2\pi r(x_B(m, n) + x_0(m_0, 0))}{M+1} \right) \right] \frac{\delta_{S,B}}{M+1}. \quad (25)$$

We recall that m and n label a given site i and the subindex 0 stands for the vacancy site (see Fig. 1). Here, armchair edges correspond to sites with $m = 1, 2$ and $m = M - 1, M$ in Fig. 1. Following Ref. 36, $n = 0$ stands for the zigzag row where the vacancy is positioned and the index increases (decreases) as one moves to rows on top (bottom), see left axis of Fig. 1. Finally, $x_B(m, n) = m/2$ (top axis of Fig. 1) indicates the transversal position on the B lattice site labeled by (m, n) .

The function $I_r(n)$ is given by³⁶

$$I_r(n) = 2(-1)^n \begin{cases} \Theta(\frac{2\pi}{3} - k_r) [2 \cos(\frac{k_r}{2})]^{-(n+1)}, & n \geq 0 \\ \Theta(k_r - \frac{2\pi}{3}) [2 \cos(\frac{k_r}{2})]^{(1-n)}, & n < 0, \end{cases} \quad (26)$$

where the “wave number” k_r obeys the quantization rule dictated by M , the finite number of sites along the transversal direction^{36,38,39} (see lower panel in Fig. 1):

$$k_r = \frac{2\pi}{M+1}r, \quad r = 1, 2, \dots, M/2, \quad (27)$$

where r is the band index. For the case where $\text{mod}(M+1, 3) \neq 0$,^{36,38,39} the nanoribbon is semiconducting, otherwise the system is metallic. In Sec. V, we use these analytical expressions for the computation of the charging energy.

We also analyze the effects of vacancies in armchair graphene nanoribbons by numerical diagonalization of the tight binding Hamiltonian $H = H_0 + V'$, see Eqs.

(2) and (4). As before, due to the lack of translational symmetry, we consider supercell with a $N_{\text{tot}} = M \times N$ sites. We use periodic boundary conditions at the zigzag chains characterized at $n = N/2$ and $n = -N/2 + 1$ (see Fig. 1).

In Fig. 3 we show the vacancy-generated state obtained from numerical diagonalization for two different vacancy-edge distances. As in the bulk, the vacancy state is pinned at zero energy^{18,19,27} and is located solely in the sublattice opposite to that of the vacancy. In Fig. 3, the black dot indicates the vacancy site. The radii of the bubbles are proportional to the amplitude of the wave functions and the blue (red) color stands for positive (negative) sign of the wave function. Note that the sites that carry the larger weights are those closer to the vacancy site.

As expected, the vacancy originates a midgap bound state pinned at zero energy.^{18,19,27} We show in the next section that this numerical approach provides results which are in very good agreement with the analytical treatment discussed above.

B. Midgap state degree of localization versus vacancy-edge distance.

Although Ref. 37 presents an extensive study of the behavior of vacancies created in semiconducting armchair ribbons, one important aspect that was not properly ex-

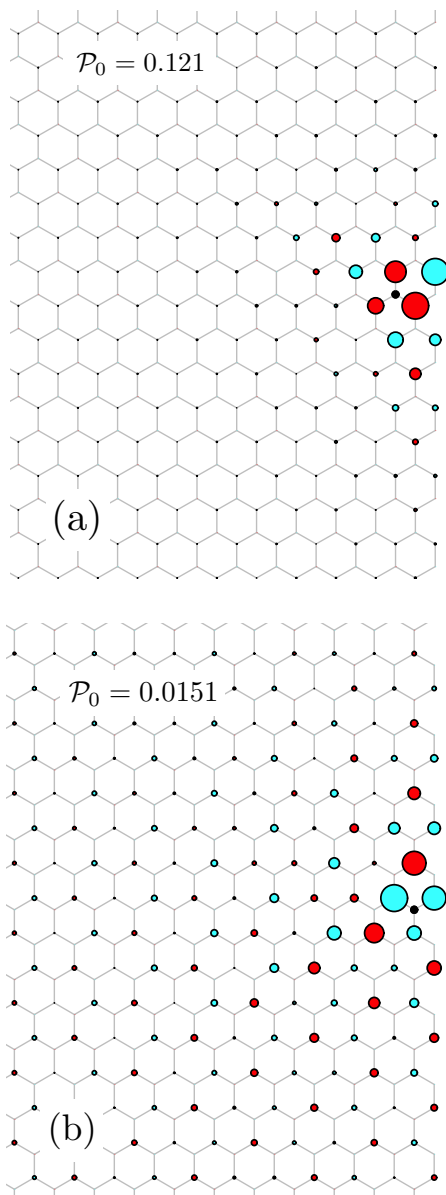


FIG. 3. (Color online) Wave function amplitudes for a vacancy at two different sites (black dots) in an armchair ribbon: (a) vacancy two sites away from the edge and (b) vacancy one site away from the edge. Note that the degree of localization drops by an order of magnitude as the vacancy is moved one site towards the edge.

explored so far is the dependency of the degree of localization of the vacancy state when the position of vacancy site is changed. Before addressing the calculation of the Coulomb charging energy for the vacancy-localized state, we discuss the nature of the localized wave functions as a function of the vacancy-edge distance D .

We characterize the degree of localization of the wave functions by the Inverse Participation Ratio (IPR) which,

for a given state of energy E_ν , reads:

$$\mathcal{P}_\nu = \sum_i |\psi_\nu(i)|^4, \quad (28)$$

The IPR is contained in the interval $(0, 1]$ and the closer to the upper (lower) limit, the higher (lower) is the degree of localization of the wave function. Note that, for the vacancy state, the $\mathcal{P}_0 = U_1/U_{\text{orbital}}$. Hence the behavior of \mathcal{P}_0 mimics the one followed by U_1 .

We find that the vacancy state is extremely sensitive to the vacancy-edge distance as shown in Fig. 3.⁶³ Figure 3a shows the midgap state for a vacancy placed two sites away from the edge ($D = 2$, in units of $a\sqrt{3}/2$). As the vacancy is moved one position towards the edge ($D = 1$, as shown in Fig. 3b), the vacancy state changes abruptly and the wave function extends much more than in the previous configuration. This behavior is qualitatively seen in Fig. 3 and quantified by the IPR. Notice that the IPRs of the two configurations differ by an order of magnitude.

Our numerical calculations show a non-monotonical decrease of the \mathcal{P}_0 as a function of the vacancy-edge distance. For very narrow ribbons, this effect is very subtle (see, for instance, the behavior of the IPR for the ribbon with width $M = 6$ in Fig. 4). For small M , the confinement due to a finite width competes with the localization due to the vacancy. Figure 4 indicates that the IPR does not depend on M for some specific sites, while for other sites the IPR decreases with increasing M . The size independent IPRs correspond to truly localized states due to the vacancy, while the others behave as quasi-localized states as those due to vacancies in bulk graphene^{19,27}. This interpretation plays a key role in our analysis and, to the best of our knowledge, has been unnoticed so far.⁶⁴

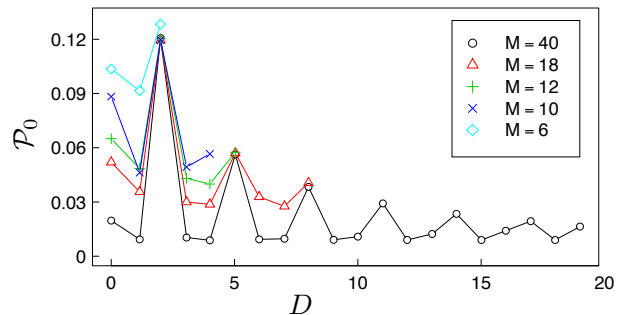


FIG. 4. (Color online) Midgap state \mathcal{P}_0 as function as a function of D , the distance of the vacancy to its closest nanoribbon edge (in units of $a\sqrt{3}/2$).

The results of Fig. 3 are obtained from numerical diagonalization with $M = N = 40$ (largest size in Fig. 4), and are consistent with the analytical approach. Figure 4 shows that \mathcal{P}_0 becomes increasingly independent of system size as the ribbon width is increased. This behavior is further confirmed by the analysis of U_1 presented in Fig. 8.

All these results are obtained for semiconducting armchair graphene nanoribbons. For metallic armchair ribbons we also find vacancy-induced states which also present the behavior observed in Figs. 3 and 4. This finding is at odds with the analysis of Ref. 36. We will return to this discussion on Sec. V where we study the behavior of U in armchair nanoribbons.

For semiconducting graphene nanoribbons, our findings for \mathcal{P}_0 can be qualitatively understood as follows. The combination of the bipartite nature of the honeycomb lattice and the presence of edges gives origin to a peculiar modulation of the degree of localization as a function of vacancy-edge distance. Some insight is provided from recent studies of the Kitaev model in the gapped phase, where it has been shown that a vacancy induces a zero mode state with a specific directionality such that the wave function of this state is nonzero only in a wedge emanating from the vacancy position and zero elsewhere.^{22,23} This directionality is only sublattice dependent, but independent from the site chosen within the same sublattice. We recall here that semiconducting armchair ribbons constitute a realization of a gapped honeycomb model.³⁸ Hence, we also observe a directionality pattern in the vacancy zero mode states in these ribbons. We note that in distinction to the Kitaev model, the systems we study have edges that strongly influence the behavior of the midgap states, particularly, their directionality and degree of localization as a function of the vacancy site position.

Further insight is obtained by inspecting the wave function with energy closest to zero of a clean armchair ribbon, illustrated in Fig. 5. By inspecting the probability of finding the states at the sites along any of the “horizontal” zigzag chains starting from the armchair edge, see Fig. 5, one clearly observes a pattern of two maxima followed by a minimum. We note that this pattern is complementary to the one we obtain for \mathcal{P}_0 as we move the vacancy across a zigzag chain. Hence, if a vacancy is placed at a site where the state closest to the zero mode of the clean ribbon has a maximum, the vacancy state suffers a larger repulsion and has to extend more, the opposite occurs when the vacancy is placed at sites with vanishing weights in the clean system.

This view is confirmed by the study of midgap states due to hydrogen adatoms (not shown here) instead of vacancies. Interestingly, the manner in which the vacancy zero mode is more localized/extended is consequence of the directionality of the midgap state. In the sites where \mathcal{P}_0 has a maximum, the vacancy state is directed towards the closest edge becoming more concentrated. In the cases where a minimum in the IPR occurs, the vacancy state is directed to the farther edges or to the ribbon’s longitudinal direction and hence becomes more extended.

This is an interesting property which could allow the tunability of a site-site entanglement²² of this system and also tune the transport properties of a specific edge due to interactions with the vacancy state. The transport along a chosen edge could be blocked or reduced just

by selecting the vacancy/adatom position respective the chosen edge. As we show in Sec. V, all these findings have a strong impact on the charging energy U .

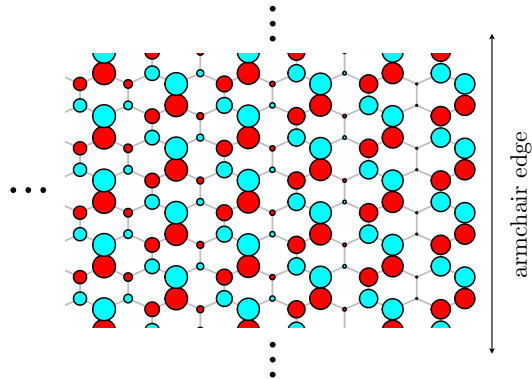


FIG. 5. (Color online) Site dependency of the amplitudes of the state with energy closest to zero energy of a pristine armchair ribbon.³⁸ The circles radii are proportional to the wave function amplitude, red and blue correspond the negative and positive amplitudes respectively.

C. Vacancies with other kinds of edges: zigzag and quantum dots

For other kinds of edges, namely zigzag, chiral and those found in quantum dots, we also observe vacancy-induced states $|\psi_0\rangle$.

For zigzag ribbons, Ref. 36 predicts that a vacancy does not affect the zero energy states of the system. Our study agrees with this result. However, we find that the vacancy gives rise to pairs of electron-hole states with same energy and amplitude (but opposite phases), as expected from chiral symmetry preservation. In addition, $|\psi_0\rangle$ clearly hybridizes with the edge-localized states of the edge with sites belonging to the opposite sublattice of the vacancy site (see Fig. 6a). These observations are in agreement with transport simulations for this kind of system.^{45,46}

The situation becomes more complicated in the case of graphene quantum dots, whose edges are (in general) a combination of zigzag and armchair chains. We find that the midgap states hybridize with the states localized at the system edges. In addition, we observe an energy shift of the vacancy state, similarly to the case of zigzag ribbons. Here the presence of the armchair-like edges also plays a role: We find a modulated behavior of the IPR of the vacancy state as the distance of the vacancy site from the armchair edge is varied. As in the case of armchair ribbons, we also observe increasing degree of localization of the vacancy state as the distance from the armchair edge is decreased. The IPR has its maximum for $D = 2$ as for armchair ribbons, see Fig. 6b.

Although we did not make an extensive numerical anal-

ysis of vacancies in zigzag ribbons or graphene quantum dots, the discussion above is useful to emphasize that the main results of our paper for the armchair ribbons should remain valid for realistic samples in which other kinds of edges and/or disorder appear.

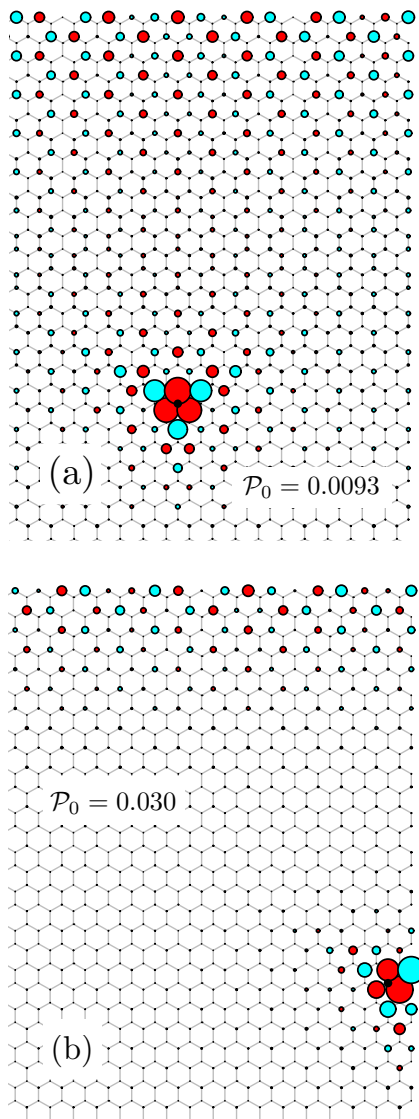


FIG. 6. Wave function amplitudes for the vacancy state in a zigzag nanoribbon (a) and for a quantum dot (b).

V. CHARGING ENERGY ESTIMATES FOR ARMCHAIR RIBBONS

We focus our attention on the analysis of vacancy-induced states in armchair graphene nanoribbons since in this case the degree of localization of the $|\psi_0\rangle$ states is much more pronounced, as discussed in the previous sections. More specifically, we calculate the charging en-

ergy U_1 and U_2 , given respectively by Eqs. (17) and (20), as a function of the vacancy-edge distance D and the nanoribbon width.

Both the analytical and the tight-binding approaches give the envelope wave functions $\psi_0(i)$ which allows one to numerically evaluate U_1 and U_2 . We compare the results and find good qualitative agreement, as shown in Fig. 7. For the cases we considered (with $M = 220$), the tight-binding values for U_1 are about 30% smaller (for the sites with the larger U_1) than those obtained using the analytical wave functions. For U_2 , which is one order of magnitude larger than U_1 , both approaches agree within 5%. In Appendix A, we provide evidence that the discrepancy is not related to the size of the supercell. We speculate that the larger discrepancy in the case of U_1 arises from the fact that it scales with the numerically-obtained amplitudes as $|\psi_0(i)|^4$ (see, e.g., Eq. (17)) while U_2 scales roughly as $|\psi_0(i)\psi_0(j)|^2$ with $i \neq j$ (Eq. (20)). Thus, the numerical values of U_1 tend to be more sensitive to small numerical errors in the calculation of the envelope wave functions $\psi_0(i)$ than those obtained for U_2 .

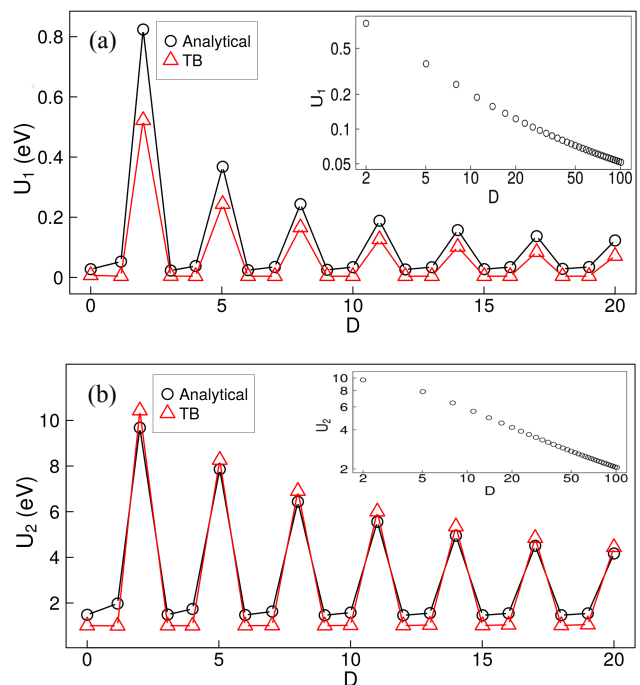


FIG. 7. (Color online) Charging energy U as a function of the vacancy-edge distance D for an armchair nanoribbon of width $M = 220$. $U = U_1 + U_2$ is calculated by using numerical and analytical wave functions. Panel (a) corresponds to the intra-atomic U_1 contribution, while (b) to the inter-atomic Coulomb term U_2 . The insets show maxima of U_1 and U_2 versus D in a log-log scale.

The calculation of U using the analytical expression for the $\psi_0(i)$ is significantly faster and demands much

less memory than the tight-binding approach, which requires storage of the Hamiltonian matrix elements. This allows us to address ribbons with micron size widths. The results presented next are obtained using analytical wave functions.

Figure 8 shows U_1 and U_2 as a function of the vacancy-edge distance D . The results clearly indicate that U is almost independent of the ribbon width M for very large systems. Moreover, for the sites for which U_1 (U_2) has a minimum, the computed charging energies approach the bulk values obtained in Fig. 2. The dependence of U_2 with D follows the same pattern as the IPR (for U_1 this is expected, since the latter is proportional to \mathcal{P}_0), namely, an oscillatory behavior as the vacancy is moved away from the edge with a fast decay in the modulation (see insets of Fig. 7). When the vacancy is far from the ribbon edges, U is suppressed with respect to its largest value by an order of magnitude and approaches the bulk estimate.

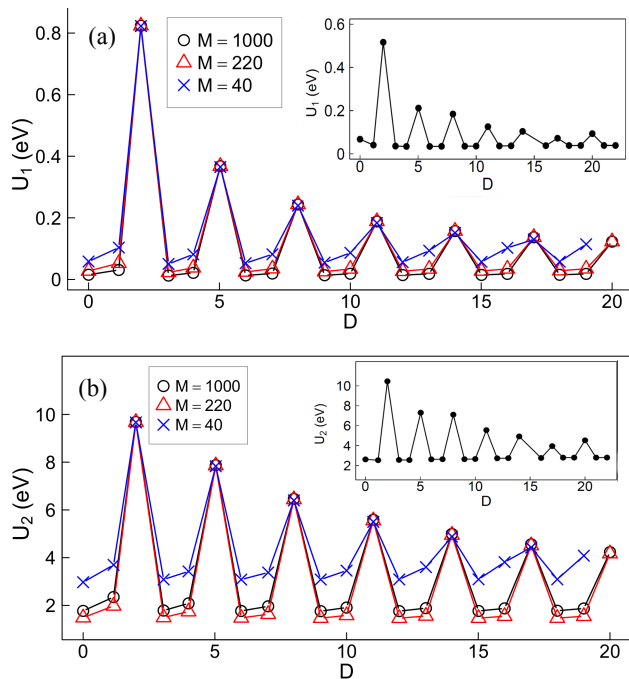


FIG. 8. (Color online) Charging energy U as a function of the vacancy-edge distance D for armchair nanoribbons of different widths, namely, $M = 40, 220$, and 1000 . The charging energy is split in an intra-atomic U_1 (a) and an inter-atomic Coulomb term U_2 (b). The insets show the tight-binding result for a metallic ribbon with $M = 44$.

We note that the ribbon with $M = 44$ is metallic. In this case, the analytical treatment of Ref. 36 predicts that the vacancy does not produce a localized state pinned at zero energy. Following the notation introduced in Ref. 36, we find that, when the vacancy is placed at the so-called nodal line (sites where the wave function of the lowest

energy state of the clean system vanishes, which correspond to the sites with the smallest probabilities in Fig. 5), a localized state pinned at zero energy arises, originating the maxima in the charging energy seen in the inset of Fig. 8 for the width $M = 44$. Interestingly, if the vacancy is placed at a site off the nodal line, we do not observe a localized state pinned at zero energy, as predicted in Ref. 36. Instead, we find that the vacancy originates an electron-hole pair of states close to zero energy with a localized character. The charging energy for these states correspond to the “minima” in the modulated pattern shown in the insets of Fig. 8. We note that these estimates are in excellent agreement with the behavior found for the semiconducting ribbons, indicating that the values for U are robust irrespective to the metallic or semiconducting character of the ribbons.

The appearance of localized states in metallic ribbons is important for the discussion of the observation of bound states immersed in the continuum (BIC) in graphene^{65,66} as the localized states here occur within a region of finite density of states.

VI. CONCLUSIONS AND OUTLOOK

In this paper we study the charging energy U , a key element to understand the magnetic properties of the system, of a localized state due to a single-vacancy in monolayer graphene bulk and in graphene nanoribbons.

We find that U can be expressed in terms of two main contributions, U_1 and U_2 , corresponding respectively to intrasite and intersite electron-electron interactions. We show that U_2 can be identified with the effective low energy expression for the Coulomb energy associated with two-dimensional electronic wave functions. Although U_2 is the dominating term, there are several scenarios where the U_1 contribution to the charging energy can become important. For instance, a recent study³⁴ suggests the use of impurities to design a lattice structure that can give rise to a graphene-based spin-liquid system. There it is argued that the onset of the spin-liquid regime depends on the ratio between the charging energy of the impurity bound state and the hopping between these impurity states,³⁴ that makes the precise assessment of U very critical to infer the system behavior.

Our systematic study of the charging energy confirms the heuristic prediction that U scales with the sample length L as $(\ln L)^{-2}$. Our estimates for U support the picture of π magnetism in realistic sample sizes, contrary to previous results.^{25,37}

Edges change significantly this simple bulk scaling. In this paper, we perform a systematic investigation of the midgap states in armchair ribbons. We establish the dependence of U and the IPR with the vacancy-edge distance and discuss how this is related to the directionality of the wave functions. Some midgap states are truly localized (unnoticed so far) with IPR and U an order of magnitude larger than the bulk value. Similar behav-

ior is also found for metallic armchair ribbons, which could be a manifestation of a BIC. This particular case is at odds with the wave function analysis presented in Ref. 36. For the remaining cases the overall agreement is very good. Moreover, we show that other kinds of edges also affect the vacancy-induced state. In particular, for zig-zag edges and quantum dots, the vacancy-induced states have energies shifted from the Dirac point due to a strong hybridization with edge-induced localized states. This observation can be an indication that our results for armchair edges can be robust in samples with edges other than zigzag and armchair.

Using the tight-binding model, we have checked that an hydrogen adatom gives raise to localized states that share some of the features of those caused by a vacancy. Their IPR, for instance, have the same oscillatory behavior we find for the armchair ribbons with vacancies. This opens the possibility of having a controlled way to verify our results by the precise manipulation of H adatoms using a STM tip and to observe the generated states pattern by a STS measurement near the adatom, as recently shown in Ref. 31. The results we present can also be checked experimentally in other platforms since they are valid for other systems with bipartite lattices. Artificial graphene could also be used to verify experimentally our findings.

We stress that a correct assessment of the substrate dielectric constant ϵ is key for a quantitative comparison of our U estimates with the experimental values. We recall that the estimates we present here were obtained considering $\epsilon = 4$ which is characteristic of graphene on top of SiO_2 .⁶¹ Depending on the dielectric environment to which graphene is exposed ϵ can vary by two orders of magnitude.⁶⁷ Hence, the dielectric media to which graphene is submitted in the recents experiments of Refs. 14 and 31, which use graphene on top of SiC and Rh substrates, respectively, can have an important influence in the discrepancies between our estimates and the observed U . A systematic experimental study of the role of the substrate and proper characterization of the dielectric constant that should be used in the U estimates is necessary to clarify this issue.

Our U estimates can be directly comparable to that of Ref. 33, which also estimates U for graphene on SiO_2 substrates. We recall that our results are 2 – 3 orders of magnitude larger than the values predicted in that paper. We note that our estimates are based on a rigorous derivation of an expression for U , whose value is computed using the (numerically precise) vacancy-state wave function amplitudes. By contrast, the values reported in Ref. 33 are based on scaling arguments for the vacancy-induced wave function, which do not take properly into account the behavior of the vacancy wave function amplitudes along the sites of the system.

Finally, we note that though the results presented for U are for single vacancies, the expression we derive is also valid for the multivacancy case. Though an analytical expression for the multivacancy wave function case

is not available in the literature, those can be obtained numerically and used to obtain U in a similar fashion as the one we use here for the single vacancy.

In summary, we present a full derivation of U for vacancy-induced localized states in graphene systems. Our results help the understanding of defect-induced carbon magnetism, allowing contact with the typical experiments that use samples with billions of atoms, where edges, multivacancies and other kinds of disorder are present, which are beyond the reach of other methods, such as DFT

ACKNOWLEDGMENTS

This work has been supported by the Brazilian funding agencies CAPES, CNPq, and FAPERJ.

Appendix A: Convergence analysis

The tight-binding model calculations are implemented using a supercell of size $M \times N$. In the case of graphene nanoribbons, M is determined by the ribbon width, while the longitudinal length N has to be conveniently chosen since the system is periodic in this direction. We optimize our calculations by choosing the smallest value of N for which U becomes independent (within less than 1%) of N .

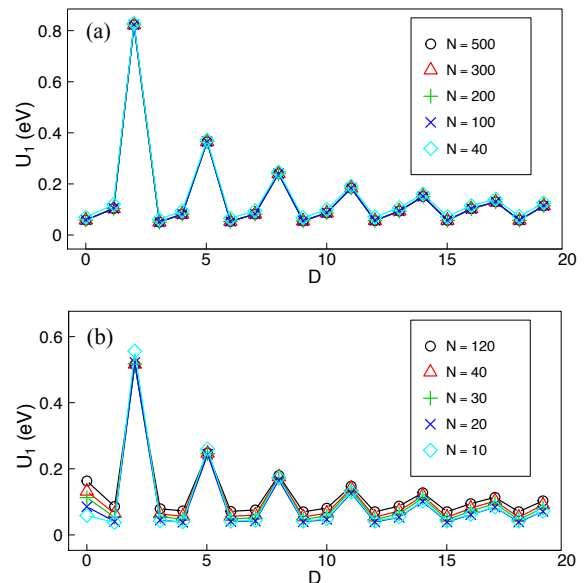


FIG. 9. (Color online) Charging energy as a function of distance for armchair ribbons with length $M = 40$ and with varying "infinite length" N . (a) Results obtained from the analytical expression of the vacancy wave function. (b) Results from the tight binding model.

In Fig. 9 we display the behavior of the U_1 as a func-

tion of edge distance D for $M = 40$ and varying N . The results are obtained by using the analytical wave function (Fig. 9a) and the tight binding model (Fig. 9b). For $M = 40$ we perform tight-binding simulations for $10 \leq N \leq 120$. For larger system sizes this method becomes computationally intensive and it is advantageous to use analytical wave functions. The calculations re-

veal that our estimates are almost independent of N and show that the results already converge for modest values of N . These calculations also indicate that the discrepancies observed in the estimates of U_1 obtained from the two approaches is not an artifact of the supercell sizes we use.

-
- ¹ A. H. Castro Neto, F. Guinea, N. M. R. Peres, K. S. Novoselov, and A. K. Geim, *Rev. Mod. Phys.* **81**, 109 (2009).
- ² A. K. Geim and K. S. Novoselov, *Nat. Mater.* **6**, 183 (2007).
- ³ K. S. Novoselov, V. I. Fal'ko, L. Colombo, P. R. Gellert, M. G. Schwab, and K. Kim, *Nature* **490**, 192 (2012).
- ⁴ J.-H. Chen, W. G. Cullen, C. Jang, M. S. Fuhrer, and E. D. Williams, *Phys. Rev. Lett.* **102**, 236805 (2009).
- ⁵ J.-H. Chen, L. Li, W. G. Cullen, E. D. Williams, and M. S. Fuhrer, *Nat. Phys.* **7**, 535 (2011).
- ⁶ R. R. Nair, M. Sepioni, I.-L. Tsai, O. Lehtinen, J. Keinonen, A. V. Krasheninnikov, T. Thomson, A. K. Geim, and I. V. Grigorieva, *Nat. Phys.* **8**, 199 (2012).
- ⁷ R. R. Nair, I.-L. Tsai, M. Sepioni, O. Lehtinen, J. Keinonen, A. V. Krasheninnikov, A. H. Castro Neto, M. I. Katsnelson, A. K. Geim, and I. V. Grigorieva, *Nat. Commun.* **4**, 2010 (2013).
- ⁸ S. Just, S. Zimmermann, V. Kataev, B. Büchner, M. Prutzer, and M. Morgenstern, *Phys. Rev. B* **90**, 125449 (2014).
- ⁹ V. W. Brar, R. Decker, H.-M. Solowan, Y. Wang, L. Maserati, K. T. Chan, H. Lee, O. Girit, A. Zettl, S. G. Louie, M. L. Cohen, and M. F. Crommie, *Nat. Phys.* **7**, 43 (2011).
- ¹⁰ M. M. Ugeda, I. Brihuega, F. Guinea, and J. M. Gómez-Rodríguez, *Phys. Rev. Lett.* **104**, 096804 (2010).
- ¹¹ M. M. Ugeda, D. Fernández-Torre, I. Brihuega, P. Pou, A. J. Martínez-Galera, R. Pérez, and J. M. Gómez-Rodríguez, *Phys. Rev. Lett.* **107**, 116803 (2011).
- ¹² J. Mao, Y. Jiang, D. Moldovan, G. Li, K. Watanabe, T. Tanigushi, M. R. Masir, F. M. Peeters, and E. Y. Andrei, *Nat. Phys.* **22**, 1745 (2016).
- ¹³ G. Lopez-Polin, C. Gomez-Navarro, V. Parente, F. Guinea, M. I. Katsnelson, F. Perez-Murano, and J. Gomez-Herrero, *Nat. Phys.* **11**, 26 (2015).
- ¹⁴ Y. Zhang, S.-Y. Li, W.-T. Li, J.-B. Qiao, W.-X. Wang, L.-J. Yin, and L. He, arXiv:1604.06542 (2016).
- ¹⁵ O. V. Yazyev, *Rep. Prog. Phys.* **73**, 56501 (2010).
- ¹⁶ V. G. Miranda, L. G. G. V. Dias da Silva, and C. H. Lewenkopf, *Phys. Rev. B* **90**, 201101 (2014).
- ¹⁷ L. Fritz and M. Vojta, *Rep. Prog. Phys.* **76**, 032501 (2012).
- ¹⁸ V. M. Pereira, F. Guinea, J. M. B. Lopes dos Santos, N. M. R. Peres, and A. H. Castro Neto, *Phys. Rev. Lett.* **96**, 036801 (2006).
- ¹⁹ V. M. Pereira, J. M. B. Lopes dos Santos, and A. H. Castro Neto, *Phys. Rev. B* **77**, 115109 (2008).
- ²⁰ S. Yuan, H. De Raedt, and M. I. Katsnelson, *Phys. Rev. B* **82**, 115448 (2010).
- ²¹ M. Inui, S. A. Trugman, and E. Abrahams, *Phys. Rev. B* **49**, 3190 (1994).
- ²² G. Santhosh, V. Sreenath, A. Lakshminarayan, and R. Narayanan, *Phys. Rev. B* **85**, 054204 (2012).
- ²³ A. J. Willans, J. T. Chalker, and R. Moessner, *Phys. Rev. B* **84**, 115146 (2011).
- ²⁴ This result holds if the A and B sublattice constituents are of the same kind. If this is not the case, the states are not pinned at $E = 0$ ¹⁹. It worth noting that vacancy zero modes in graphene can also be generated even if $N_A = N_B$ as long as the system is composed of clusters for which $N_A \neq N_B$ inside the cluster^{37,68}.
- ²⁵ J. J. Palacios and F. Ynduráin, *Phys. Rev. B* **85**, 245443 (2012).
- ²⁶ C.-C. Lee, Y. Yamada-Takamura, and T. Ozaki, *Phys. Rev. B* **90**, 014401 (2014).
- ²⁷ B. R. K. Nanda, M. Sherafati, Z. S. Popović, and S. Satpathy, *New J. Phys.* **14**, 83004 (2012).
- ²⁸ M. Casartelli, S. Casolo, G. F. Tantardini, and R. Martignazzo, *Phys. Rev. B* **88**, 195424 (2013).
- ²⁹ P. Francis, C. Majumder, and S. Ghaisas, *Carbon* **91**, 358 (2015).
- ³⁰ W. S. Paz, W. L. Scopel, and J. C. C. Freitas, *Solid State Commun.* **175 - 176**, 71 (2013).
- ³¹ H. Gonzalez-Herrero, J. M. Gomez-Rodriguez, P. Mallet, M. Moaied, J. J. Palacios, C. Salgado, M. M. Ugeda, J.-Y. Veuillen, F. Yndurain, and I. Brihuega, *Science* **352**, 437 (2016).
- ³² E. H. Lieb, *Phys. Rev. Lett.* **62**, 1201 (1989).
- ³³ M. A. Cazalilla, A. Iucci, F. Guinea, and A. H. Castro Neto, cond-mat/1207.3135 (2012).
- ³⁴ X. Dou, V. N. Kotov, and B. Uchoa, arXiv:1602.01477 (2016).
- ³⁵ H.-Y. Deng and K. Wakabayashi, *Phys. Rev. B* **90**, 115413 (2014).
- ³⁶ H.-Y. Deng and K. Wakabayashi, *Phys. Rev. B* **91**, 035425 (2015).
- ³⁷ J. J. Palacios, J. Fernández-Rossier, and L. Brey, *Phys. Rev. B* **77**, 195428 (2008).
- ³⁸ L. Brey and H. A. Fertig, *Phys. Rev. B* **73**, 235411 (2006).
- ³⁹ H. Zheng, Z. F. Wang, T. Luo, Q. W. Shi, and J. Chen, *Phys. Rev. B* **75**, 165414 (2007).
- ⁴⁰ E. R. Mucciolo, A. H. Castro Neto, and C. H. Lewenkopf, *Phys. Rev. B* **79**, 075407 (2009).
- ⁴¹ A. R. Carvalho, J. H. Warnes, and C. H. Lewenkopf, *Phys. Rev. B* **89**, 245444 (2014).
- ⁴² C. Tao, L. Jiao, O. V. Yazyev, Y.-C. Chen, J. Feng, X. Zhang, R. B. Capaz, J. M. Tour, A. Zettl, S. G. Louie, H. Dai, and M. F. Crommie, *Nat. Phys.* **7**, 616 (2011).
- ⁴³ G. Z. Magda, X. Jin, I. Hagymasi, P. Vancso, Z. Osvath, P. Nemes-Incze, C. Hwang, L. P. Biro, and L. Tapasztó, *Nature* **514**, 608 (2014).
- ⁴⁴ S. Wang, L. Talirz, C. A. Pignedoli, X. Feng, K. Muellen, R. Fasel, and P. Ruffieux, ArXiv e-prints (2015), arXiv:1511.04940 [cond-mat.mtrl-sci].
- ⁴⁵ D. A. Bahamon, A. L. C. Pereira, and P. A. Schulz, *Phys.*

- Rev. B **82**, 165438 (2010).
- ⁴⁶ A. Orlof, J. Ruseckas, and I. V. Zozoulenko, *Phys. Rev. B* **88**, 125409 (2013).
- ⁴⁷ N. Gorjizadeh, A. A. Farajian, and Y. Kawazoe, *Nanotechnology* **20**, 15201 (2009).
- ⁴⁸ D. Midtvedt and A. Croy, *J. Phys.: Condens. Matter* **28**, 045302 (2016).
- ⁴⁹ M. Schüler, M. Rösner, T. O. Wehling, A. I. Lichtenstein, and M. I. Katsnelson, *Phys. Rev. Lett.* **111**, 036601 (2013).
- ⁵⁰ E. N. Economou, *Green's Functions in Quantum Physics*, 3rd ed. (Springer, Berlin, 2006).
- ⁵¹ E. Kaxiras, *Atomic and Electronic Structure of Solids*, 1st ed. (Cambridge University Press, Cambridge, 2003).
- ⁵² A. Zunger and R. Englman, *Phys. Rev. B* **17**, 642 (1978).
- ⁵³ W. Ku, T. Berlijn, and C.-C. Lee, *Phys. Rev. Lett.* **104**, 216401 (2010).
- ⁵⁴ M. E. A. Coury, S. L. Dudarev, W. M. C. Foulkes, A. P. Horsfield, P.-W. Ma, and J. S. Spencer, *Phys. Rev. B* **93**, 075101 (2016).
- ⁵⁵ W. A. Harrison, *Phys. Rev. B* **31**, 2121 (1985).
- ⁵⁶ C. M. Goringe, D. R. Bowler, and E. Hernández, *Rep. Prog. Phys.* **60**, 1447 (1997).
- ⁵⁷ M. Elstner, D. Porezag, G. Jungnickel, J. Elsner, M. Haugk, T. Frauenheim, S. Suhai, and G. Seifert, *Phys. Rev. B* **58**, 7260 (1998).
- ⁵⁸ R. G. Parr, D. P. Craig, and I. G. Ross, *J. Chem. Phys.* **18**, 1561 (1950).
- ⁵⁹ T. O. Wehling, E. Şaşıoğlu, C. Friedrich, A. I. Lichtenstein, M. I. Katsnelson, and S. Blügel, *Phys. Rev. Lett.* **106**, 236805 (2011).
- ⁶⁰ Our approximation is also consistent with the ratios between U_{01} , U_{02} , and U_{03} (bare) reported in Ref. 59.
- ⁶¹ C.-P. Lu, G. Li, K. Watanabe, T. Taniguchi, and E. Y. Andrei, *Phys. Rev. Lett.* **113**, 156804 (2014).
- ⁶² D. Soriano, D. Van Tuan, S. M-M Dubois, M. Gmitra, A. W. Cummings, D. Kochan, F. Ortman, J.-C. Charlier, J. Fabian, and S. Roche, *2D Materials* **2**, 022002 (2015).
- ⁶³ On the other hand, we find that when the vacancy state is moved in the direction parallel the edges, the degree of localization is unchanged, which is quite reasonable since the system is “infinite” in this direction.
- ⁶⁴ The latter states were probably the states observed in Refs. 37 and 48 which led them to conclude that going from a very narrow ribbon to bulk graphene would turn the localized state into a non-normalizable one with vanishing spin splitting for the midgap state. Hence, a vanishing magnetization.
- ⁶⁵ J. W. González, M. Pacheco, L. Rosales, and P. A. Orellana, *EPL (Europhysics Letters)* **91**, 66001 (2010).
- ⁶⁶ N. Cortés, L. Chico, M. Pacheco, L. Rosales, and P. A. Orellana, *EPL (Europhysics Letters)* **108**, 46008 (2014).
- ⁶⁷ V. N. Kotov, B. Uchoa, V. M. Pereira, F. Guinea, and A. H. Castro Neto, *Rev. Mod. Phys.* **84**, 1067 (2012).
- ⁶⁸ N. Weik, J. Schindler, S. Bera, G. C. Solomon, and F. Evers, ArXiv e-prints (2016), [arXiv:1603.00212 \[cond-mat.dis-nn\]](https://arxiv.org/abs/1603.00212).